Letter

# Polarized structure function $\sigma_{LT'}$ from $\pi^0 p$ electroproduction data in the resonance region at $0.4\,\mathrm{GeV}^2 < Q^2 < 1.0\,\mathrm{GeV}^2$

E. L. Isupov,[36,7] V. D. Burkert,[39] A. A. Golubenko,[36] K. Joo,[7] N. S. Markov,[39,7] V. I. Mokeev,[39] L. C. Smith,[46] W. R. Armstrong,[1] H. Atac,[38] H. Avakian,[39] N. A. Baltzell,[39] L. Barion,[14] M. Battaglieri,[39,16] I. Bedlinskiy,[26] F. Benmokhtar,[8] A. Bianconi,[41,20] L. Biondo,[16,19,42] A. S. Biselli,[9,3] M. Bondi,[16] F. Bossù,[5] W. J. Briscoe,[13] W. K. Brooks,[40,39] D. Bulumulla,[31] R. A. Capobianco,[7] D. S. Carman,[39] J. C. Carvajal,[11] P. Chatagnon,[21] V. Chesnokov,[36] G. Ciullo,[14,10] P. L. Cole,[24,39] B. A. Clary,[51,7] M. Contalbrigo,[14] G. Costantini,[41,20] A. D'Angelo,[17,35] N. Dashyan,[48] R. De Vita,[16] M. Defurne,[5] A. Deur,[39] S. Diehl,[32,7] C. Djalali,[30,37] R. Dupre,[21] H. Egiyan,[39] A. El Alaoui,[40] L. El Fassi,[25] L. Elouadrhiri,[39] P. Eugenio,[12] S. Fegan,[44] A. Filippi,[18] G. Gavalian,[39,27] G. P. Gilfoyle,[34] D. I. Glazier,[43] R. W. Gothe,[37] K. A. Griffioen,[47] M. Guidal,[21] L. Guo,[11] K. Hafidi,[1] H. Hakobyan,[40,48] M. Hattawy,[31] T. B. Hayward,[7] D. Heddle,[6,39] K. Hicks,[30] A. Hobart,[21] M. Holtrop,[27] I. Illari,[13] D. G. Ireland,[43] D. Jenkins,[45] H. S. Jo,[23] D. Keller,[46] A. Khanal,[11] M. Khandaker,[29,*] A. Kim,[7] W. Kim,[23] F. J. Klein,[4] V. Klimenko,[7] A. Kripko,[32] V. Kubarovsky,[39,33] V. Lagerquist,[31] L. Lanza,[17] M. Leali,[41,20] P. Lenisa,[14,10] K. Livingston,[43] I. J. D. MacGregor,[43] D. Marchand,[21] L. Marsicano,[16] V. Mascagna,[41,20] B. McKinnon,[43] Z. E. Meziani,[1] S. Migliorati,[41,20] T. Mineeva,[40] M. Mirazita,[15] C. Munoz Camacho,[21] P. Nadel-Turonski,[39] K. Neupane,[37] S. Niccolai,[21,13] T. O'Connell,[7] M. Osipenko,[16] P. Pandey,[31] M. Paolone,[28] L. L. Pappalardo,[14,10] R. Paremuzyan,[39] E. Pasyuk,[39] S. J. Paul,[49] W. Phelps,[6] N. Pilleux,[21] O. Pogorelko,[26] J. Poudel,[31] J. W. Price,[2] Y. Prok,[31,46] B. A. Raue,[11] T. Reed,[11] M. Ripani,[16] J. Ritman,[22] J. Rowley,[30] F. Sabatié,[5] C. Salgado,[29] A. Schmidt,[13] R. A. Schumacher,[3] Y. G. Sharabian,[39] E. V. Shirokov,[36] U. Shrestha,[7] P. Simmerling,[7] D. Sokhan,[5,43] N. Sparveris,[38] S. Stepanyan,[39] I. I. Strakovsky,[13] S. Strauch,[37,13] J. A. Tan,[23] R. Tyson,[43] M. Ungaro,[39,33] S. Vallarino,[14] L. Venturelli,[41,20] H. Voskanyan,[48] E. Voutier,[21] D. Watts,[44] K. Wei,[7] X. Wei,[39] M. H. Wood,[50] B. Yale,[47] N. Zachariou,[44] J. Zhang,[46] and V. Ziegler[39]

(CLAS Collaboration)

[1]*Argonne National Laboratory, Argonne, Illinois 60439, USA*
[2]*California State University, Dominguez Hills, Carson, California 90747, USA*
[3]*Carnegie Mellon University, Pittsburgh, Pennsylvania 15213, USA*
[4]*Catholic University of America, Washington, D.C. 20064, USA*
[5]*IRFU, CEA, Université Paris-Saclay, F-91191 Gif-sur-Yvette, France*
[6]*Christopher Newport University, Newport News, Virginia 23606, USA*
[7]*University of Connecticut, Storrs, Connecticut 06269, USA*
[8]*Duquesne University, 600 Forbes Avenue, Pittsburgh, Pennsylvania 15282, USA*
[9]*Fairfield University, Fairfield, Connecticut 06824, USA*
[10]*Universita' di Ferrara, 44121 Ferrara, Italy*
[11]*Florida International University, Miami, Florida 33199, USA*
[12]*Florida State University, Tallahassee, Florida 32306, USA*
[13]*The George Washington University, Washington, D.C. 20052, USA*
[14]*INFN, Sezione di Ferrara, 44100 Ferrara, Italy*
[15]*INFN, Laboratori Nazionali di Frascati, 00044 Frascati, Italy*
[16]*INFN, Sezione di Genova, 16146 Genova, Italy*
[17]*INFN, Sezione di Roma Tor Vergata, 00133 Rome, Italy*
[18]*INFN, Sezione di Torino, 10125 Torino, Italy*
[19]*INFN, Sezione di Catania, 95123 Catania, Italy*
[20]*INFN, Sezione di Pavia, 27100 Pavia, Italy*
[21]*Universit'e Paris-Saclay, CNRS/IN2P3, IJCLab, 91405 Orsay, France*
[22]*Institute fur Kernphysik (Juelich), Juelich, Germany*
[23]*Kyungpook National University, Daegu 41566, Republic of Korea*
[24]*Lamar University, 4400 MLK Blvd, PO Box 10046, Beaumont, Texas 77710, USA*
[25]*Mississippi State University, Mississippi State, Mississippi 39762-5167, USA*
[26]*National Research Centre Kurchatov Institute - ITEP, Moscow, 117259, Russia*
[27]*University of New Hampshire, Durham, New Hampshire 03824-3568, USA*
[28]*New Mexico State University, P.O. Box 30001, Las Cruces, New Mexico 88003, USA*
[29]*Norfolk State University, Norfolk, Virginia 23504, USA*
[30]*Ohio University, Athens, Ohio 45701, USA*
[31]*Old Dominion University, Norfolk, Virginia 23529, USA*

[*]Current address: Idaho State University, Pocatello, Idaho 83209, USA.

 

[32]*II Physikalisches Institut der Universitaet Giessen, 35392 Giessen, Germany*
[33]*Rensselaer Polytechnic Institute, Troy, New York 12180-3590, USA*
[34]*University of Richmond, Richmond, Virginia 23173, USA*
[35]*Universita' di Roma Tor Vergata, 00133 Rome Italy*
[36]*Skobeltsyn Institute of Nuclear Physics, Lomonosov Moscow State University, 119234 Moscow, Russia*
[37]*University of South Carolina, Columbia, South Carolina 29208, USA*
[38]*Temple University, Philadelphia, Pennsylvania 19122, USA*
[39]*Thomas Jefferson National Accelerator Facility, Newport News, Virginia 23606, USA*
[40]*Universidad Técnica Federico Santa María, Casilla 110-V Valparaíso, Chile*
[41]*Università degli Studi di Brescia, 25123 Brescia, Italy*
[42]*Universit'a degli Studi di Messina, 98166 Messina, Italy*
[43]*University of Glasgow, Glasgow G12 8QQ, United Kingdom*
[44]*University of York, York YO10 5DD, United Kingdom*
[45]*Virginia Tech, Blacksburg, Virginia 24061-0435, USA*
[46]*University of Virginia, Charlottesville, Virginia 22901, USA*
[47]*College of William and Mary, Williamsburg, Virginia 23187-8795, USA*
[48]*Yerevan Physics Institute, 375036 Yerevan, Armenia*
[49]*University of California, Riverside, California, 92521, USA*
[50]*Canisius College, Buffalo, New York, USA*
[51]*Lawrence Livermore National Laboratory, Livermore, California 94550, USA*

(Received 25 December 2021; accepted 31 January 2022; published 18 February 2022)

The first results on the $\sigma_{LT'}$ structure function in exclusive $\pi^0 p$ electroproduction at invariant masses of the final state of 1.5 GeV $< W <$ 1.8 GeV and in the range of photon virtualities 0.4 GeV$^2$ $< Q^2 <$ 1.0 GeV$^2$ were obtained from data on beam spin asymmetries and differential cross sections measured with the CLAS detector at Jefferson Lab. The Legendre moments determined from the $\sigma_{LT'}$ structure function have demonstrated sensitivity to the contributions from the nucleon resonances in the second and third resonance regions. These new data on the beam spin asymmetries in $\pi^0 p$ electroproduction extend the opportunities for the extraction of the nucleon resonance electro-excitation amplitudes in the mass range above 1.6 GeV.

DOI: 10.1103/PhysRevC.105.L022201

Studies of $\pi N$ electroproduction are an effective tool for the exploration of nucleon resonance structure [1–5]. The CEBAF Large Acceptance Spectrometer (CLAS) at Jefferson Lab has provided most of the available information on these electroproduction channels at invariant masses of the final-state hadrons $W < 1.8$ GeV and at photon virtualities $Q^2 <$ 5.0 GeV$^2$ [6–10]. The available data allow us to determine the nucleon resonance electro-excitation amplitudes (i.e., the $\gamma_v pN^*$ electrocouplings) for most resonances over this kinematic range [1,2,5,9]. These results allow us to evaluate the resonant contribution to inclusive electron scattering with the $\gamma_v pN^*$ electrocouplings available from the experimental data, thereby paving the way to gain insight into the parton distributions in the ground-state nucleon within the resonance excitation region [11,12]. High-level analyses of the results on the $\gamma_v pN^*$ electrocouplings have revealed the structure of nucleon resonances as a complex interplay between the inner core of three dressed quarks and an external meson baryon cloud [1–3], shed light on the emergence of hadron mass [1,4,13,14], and allow for the modeling of $N^*$ structure within different quark models [15–20].

CLAS studies of $\pi^+ n$ electroproduction [9] have provided the $\gamma_v pN^*$ electrocouplings for the $N(1675)5/2^-$, $N(1680)5/2^+$, and $N(1710)1/2^+$ resonances [15]. For a complete isospin analysis, it is important to explore both the $\pi^+ n$ and $\pi^0 p$ channels. Recently, new CLAS results on the differential $\pi^0 p$ electroproduction cross sections have become available for $W < 1.8$ GeV and 0.4 GeV$^2$ $< Q^2 <$ 1.0 GeV$^2$ [10]. However, the data on $\pi N$ electroproduction at $W > 1.6$ GeV and $Q^2 < 1.0$ GeV$^2$ consist mostly of measurements with an unpolarized electron beam and an unpolarized proton target.

Measurement of the beam spin asymmetry (BSA) and the related $\sigma_{LT'}$ structure function can provide important constraints on the extraction of the $\gamma_v pN^*$ electrocouplings when combined with the differential cross sections. The $\sigma_{LT'}$ structure function determines the imaginary part of bilinear products between longitudinal and transverse amplitudes. Small contributions from the imaginary part of the longitudinal resonance amplitudes are amplified in their interference with the real part of the nonresonant contributions, making the BSAs an important observable for extraction of the longitudinal $S_{1/2}$ $\gamma_v pN^*$ electrocouplings. Previous studies of BSAs in both the $\pi^+ n$ and $\pi^0 p$ channels [21–24] were focused in the range of $W < 1.5$ GeV. They demonstrated a substantial impact of the BSA data on the extraction of the $\Delta(1232)3/2^+$ and $N(1440)1/2^+$ $S_{1/2}$ electrocouplings published in Ref. [5].

In this Letter, we present new measurements of the BSAs and $\sigma_{LT'}$ structure function from the CLAS $\pi^0 p$ electroproduction data with a major focus on the exploration of the

second and third resonance regions. The data reported here cover the kinematic area of 1.5 GeV $< W <$ 1.8 GeV and 0.4 GeV$^2$ $< Q^2 <$ 1.0 GeV$^2$ with the full angular range in the center-of-mass (CM) frame.

The data were taken during the e1e run period with the CLAS detector [25]. A longitudinally polarized electron beam of 2.036-GeV energy and 10-nA nominal current was incident on a 2-cm-long liquid-hydrogen ($LH_2$) target. The beam polarization determined from Møller polarimeter measurements was $78.9 \pm 2.8(\text{stat}) \pm 3.0(\text{syst})\%$. All details on particle identification, event selection, and the related systematic uncertainties are available in our previous publication on $\pi^0 p$ cross sections and exclusive structure functions [10].

The kinematics of the $ep \to e'\pi^0 p$ reaction can be fully described by $Q^2$, $W$, and the final-state pion polar $\theta_\pi$ and azimuthal $\phi_\pi$ emission angles in the CM frame, where $\phi_\pi$ is defined relative to the electron-scattering plane. The exclusive $\pi^0 p$ events were identified from the missing mass squared $M_X^2$ distributions in the reaction $ep \to e'pX$ after application of kinematic cuts to eliminate Bethe-Heitler backgrounds [10]. The exclusivity cuts over $M_X^2$ were applied in three-dimensional bins of $(Q^2, W, \cos\theta_\pi)$. The selected $\pi^0 p$ events were binned using a $(Q^2, W, \cos\theta_\pi, \phi_\pi)$ grid consisting of two bins over $Q^2$: from 0.4 GeV$^2$ to 0.6GeV$^2$ and from 0.6GeV$^2$ to 1.0 GeV$^2$, 28 bins over $W$, 10 bins over $\cos\theta_\pi$, and 12 bins over $\phi_\pi$ of equal sizes.

The measured asymmetry $A_{LT'}(Q^2, W, \cos\theta_\pi, \phi_\pi)$ was obtained from the event yields produced by the incoming electrons of positive and negative helicities, $N_\pi^+(Q^2, W, \cos\theta_\pi, \phi_\pi)$ and $N_\pi^-(Q^2, W, \cos\theta_\pi, \phi_\pi)$:

$$A_{LT'} = \frac{1}{P_e}\frac{(N_\pi^+ - N_\pi^-)}{(N_\pi^+ + N_\pi^-)}, \tag{1}$$

where $P_e$ is the electron-beam polarization. Representative examples of the BSA in the $ep \to e'\pi^0 p$ reaction at $W$ values in the second and third resonance regions are shown in Fig. 1. The full set of BSA data from our measurement is available in the CLAS Physics Database [26]. The data in Fig. 1 are compared with the MAID model [27] predictions for the BSA computed with the $\gamma_v pN^*$ electrocouplings from CLAS analyses of $\pi N$ and $\pi^+\pi^- p$ data [5,11,15,28,29] and MAID analyses [30] of the $\pi N$ electroproduction data. The BSAs predicted with the resonance electrocouplings from both the CLAS and MAID analyses are consistent in the second resonance region and reasonably reproduce the BSA data [see Fig. 1 (top)], demonstrating consistency of the MAID and CLAS analysis results on resonance electro-excitation in the second resonance region. In the third resonance region the BSAs computed with the CLAS and MAID results on the $\gamma_v pN^*$ electrocouplings are substantially different. Our results will be essential to improve the knowledge on the $\gamma_v pN^*$ electrocouplings of the resonances in the third resonance region.

The $\gamma_v p \to \pi^0 p$ virtual photon differential cross sections $\frac{d\sigma}{d\Omega_\pi}(Q^2, W, \cos\theta_\pi, \phi_\pi)$ for an electron beam of helicity $h$ $(h = \pm 1)$ off unpolarized protons depends on five structure functions. The transverse $\sigma_T(Q^2, W, \cos\theta_\pi)$, the longitudinal $\sigma_L(Q^2, W, \cos\theta_\pi)$, the transverse-transverse $\sigma_{TT}(Q^2, W, \cos\theta_\pi)$, and the longitudinal-transverse

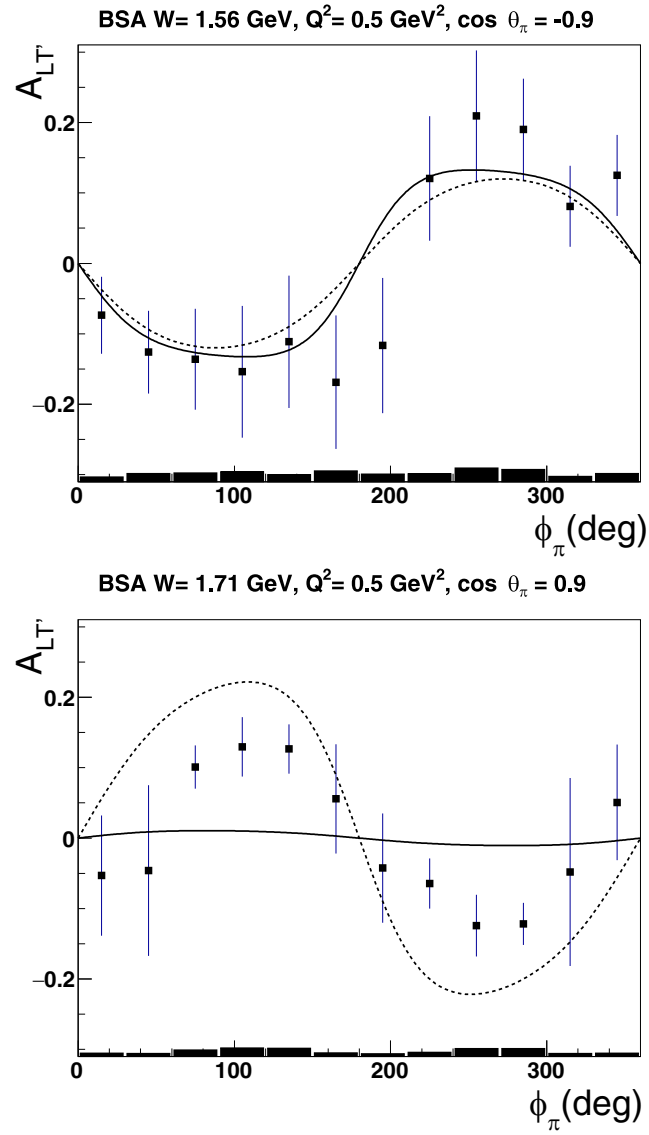


FIG. 1. BSA as a function of the CM pion azimuthal angle $\phi_\pi$ for the $ep \to e'\pi^0 p$ reaction at $W = 1.56$ GeV, $Q^2 = 0.5$ GeV$^2$, $\cos\theta_\pi = -0.9$ (top) and at $W = 1.71$ GeV, $Q^2 = 0.5$ GeV$^2$, $\cos\theta_\pi = 0.9$ (bottom). The MAID model [27] expectation with the $\gamma_v pN^*$ electrocouplings from MAID [30] and the CLAS analyses [11,28,29] are shown by the solid and dotted lines, respectively.

$\sigma_{LT}(Q^2, W, \cos\theta_\pi)$ structure functions describe the helicity-independent part of the differential cross section, while the part proportional to the electron-beam helicity $h$ is described by the $\sigma_{LT'}(Q^2, W, \cos\theta_\pi)$ structure function [27]:

$$\frac{d\sigma}{d\Omega_\pi} = \frac{p_\pi^*}{k_\gamma^*}(\sigma_0 + h\sqrt{2\epsilon_L(1-\epsilon)}\,\sigma_{LT'}\,\sin\theta_\pi\,\sin\phi_\pi),$$
$$\sigma_0 = \sigma_T + \epsilon_L\sigma_L + \epsilon\,\sigma_{TT}\,\sin^2\theta_\pi\,\cos 2\phi_\pi + \sqrt{2\epsilon_L(1+\epsilon)}\,\sigma_{LT}\,\sin\theta_\pi\,\cos\phi_\pi, \tag{2}$$

where $p_\pi^*$ is the magnitude of the $\pi^0$ momentum in the CM frame. The commonly used real photon equivalent energy $k_\gamma^*$

and the virtual photon polarization parameters $\epsilon$ and $\epsilon_L$ are described in Ref. [27].

Determination of $\sigma_{LT'}$ was made through the BSA $A_{LT'}$ and a parametrization of the $\sigma_0$ cross sections from the previous measurement [10]:

$$A_{LT'} = \frac{\sqrt{2\epsilon_L(1-\epsilon)}\,\sigma_{LT'}\,\sin\theta_\pi\,\sin\phi_\pi}{\sigma_0}. \tag{3}$$

The $A_{LT'}$ values are multiplied by $\sigma_0$ and the structure function $\sigma_{LT'}$ was then extracted using Eq. (3) through fitting the $\phi_\pi$ distributions in each bin of $(Q^2, W, \cos\theta_\pi)$. The systematic uncertainties of $\sigma_{LT'}$ are less than 10% and arise mainly from the uncertainties of the beam polarization $P_e$ and the uncertainties of $\sigma_0$ from the available measurements [10]. The contributions from the systematic uncertainties for the BSAs are much smaller and were not included in the evaluation of the systematic uncertainties for $\sigma_{LT'}$. Representative examples of the structure functions $\sigma_{LT'}$ at $W > 1.6$ GeV are shown in Fig. 2. The full set of our results for $\sigma_{LT'}$ can be found in Ref. [26].

Results on the $\sigma_{LT'}$ structure function for $\pi^0 p$ electroproduction in the third resonance region are presented here for the first time. In Fig. 2 we also show the comparison between the data on $\sigma_{LT'}$ from our measurements and the expectations from MAID [27]. This unitarized reaction model incorporates all well-established resonances parametrized using Breit-Wigner amplitudes and with backgrounds calculated from $t$-channel vector-meson exchange and other Born diagrams. The $\sigma_{LT'}$ are computed with the $\gamma_v pN^*$ resonance electrocouplings obtained from the analyses of the $\pi N$ electroproduction channels only [30] and from the CLAS $\pi N$ and $\pi^+\pi^- p$ electroproduction data [11,28,29].

To explore the sensitivity of $\sigma_{LT'}$ to the contributions from nucleon resonances ($N^*$), we decomposed this structure function using a Legendre polynomial expansion for each bin of $(Q^2, W)$ to determine the Legendre moments $D_l(Q^2, W)$:

$$\sigma_{LT'} = \sum_{\ell=0}^{\ell_{\max}} D_\ell P_\ell(\cos\theta_\pi), \tag{4}$$

with $l$ from zero to three. The expansion of Eq. (4) is truncated at $l_{\max} = 3$ to provide a stable description of the $\cos\theta_\pi$ dependence of $\sigma_{LT'}$. The results on the $W$ dependence of the Legendre moments $D_l$ are shown in Fig. 3. The full set of extracted Legendre moments is available in Ref. [26].

To relate the Legendre moments $D_l$ to the bilinear products of the $\pi^0 p$ multipole electroproduction amplitudes, the formalism developed in Ref. [31] is used. The $\sigma_{LT'}$ structure function is expressed in terms of bilinear combinations of the $F_i$ CGLN amplitudes, as described in Appendix C of Ref. [31]. Eqs. (23)–(28) in that paper allow us to relate the CGLN amplitudes $F_i$ $(i = 1, \ldots, 6)$ to the bilinear products of the multipole amplitudes that enter into the $D_l$ Legendre moments. Since the bilinear product of multipoles in the Legendre moments $D_l$ of different $l$ values contain the contributions from resonances of different spins and parities, the Legendre moments $D_l$ are suitable for disentangling the electro-excitation of different nucleon resonances.

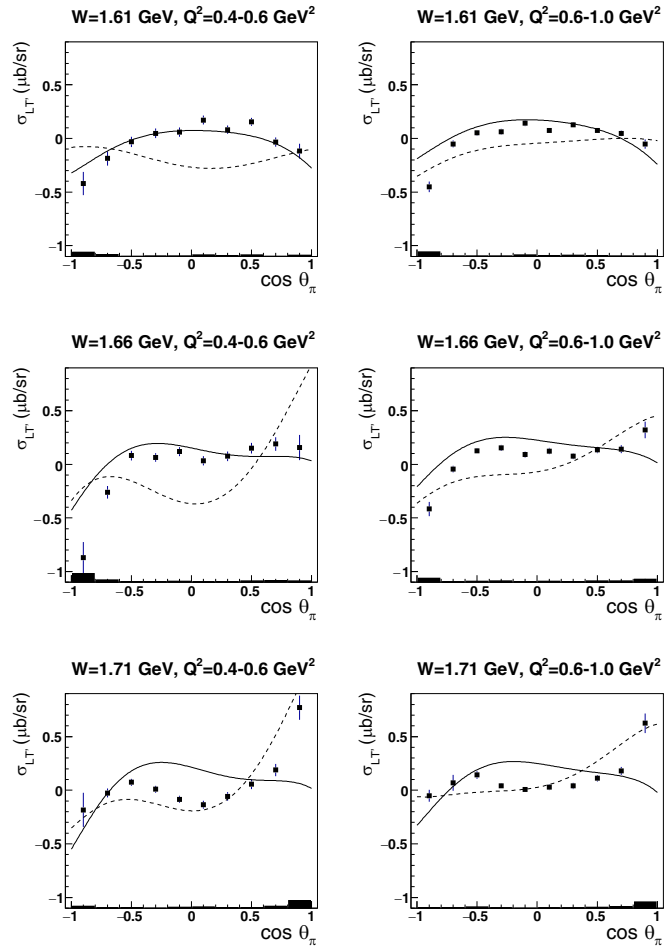


FIG. 2. The structure function $\sigma_{LT'}$ for $\pi^0 p$ electroproduction off protons at $W > 1.6$ GeV, $Q^2$ from 0.4 GeV$^2$ to 0.6 GeV$^2$ (left panel) and from 0.6 GeV$^2$ to 1.0 GeV$^2$ (right panel). The lines represent the evaluations within the MAID reaction model [27] with the $\gamma_v pN^*$ electrocouplings from the $\pi N$ electroproduction analysis [30] (solid line) and from the CLAS exclusive meson electroproduction data analyses (dashed line) [11,28,29]. The systematic uncertainties on the data are shown by the shadowed areas at the bottom of each plot.

We explored the sensitivity of the $D_l$ Legendre moments to the variation of the $\gamma_v pN^*$ electrocouplings of all pronounced resonances in the second and third resonance regions and, in particular, to the $\Delta(1620)1/2^-$, $\Delta(1700)3/2^-$, and $N(1720)3/2^+$ electrocouplings that currently have been established from solely the $\pi^+\pi^- p$ electroproduction data. The sensitivity of the $D_l$ moments to the variation of the electrocouplings of all prominent resonances can be demonstrated by computing them within the MAID model [27] with the $\gamma_v pN^*$ electrocouplings from only the $\pi N$ electroproduction data [30] and from the CLAS results [11,28,29] on the $\gamma_v pN^*$ electrocouplings determined from both $\pi N$ and $\pi^+\pi^- p$ electroproduction, as shown by the thick solid and dashed lines in Fig. 3, respectively. The sensitivity of the $D_l$ moments to the contribution from each of the states $\Delta(1620)1/2^-$, $\Delta(1700)3/2^-$ and $N(1720)3/2^+$ was studied by turning off each in turn while taking the $\gamma_v pN^*$ electrocouplings of the

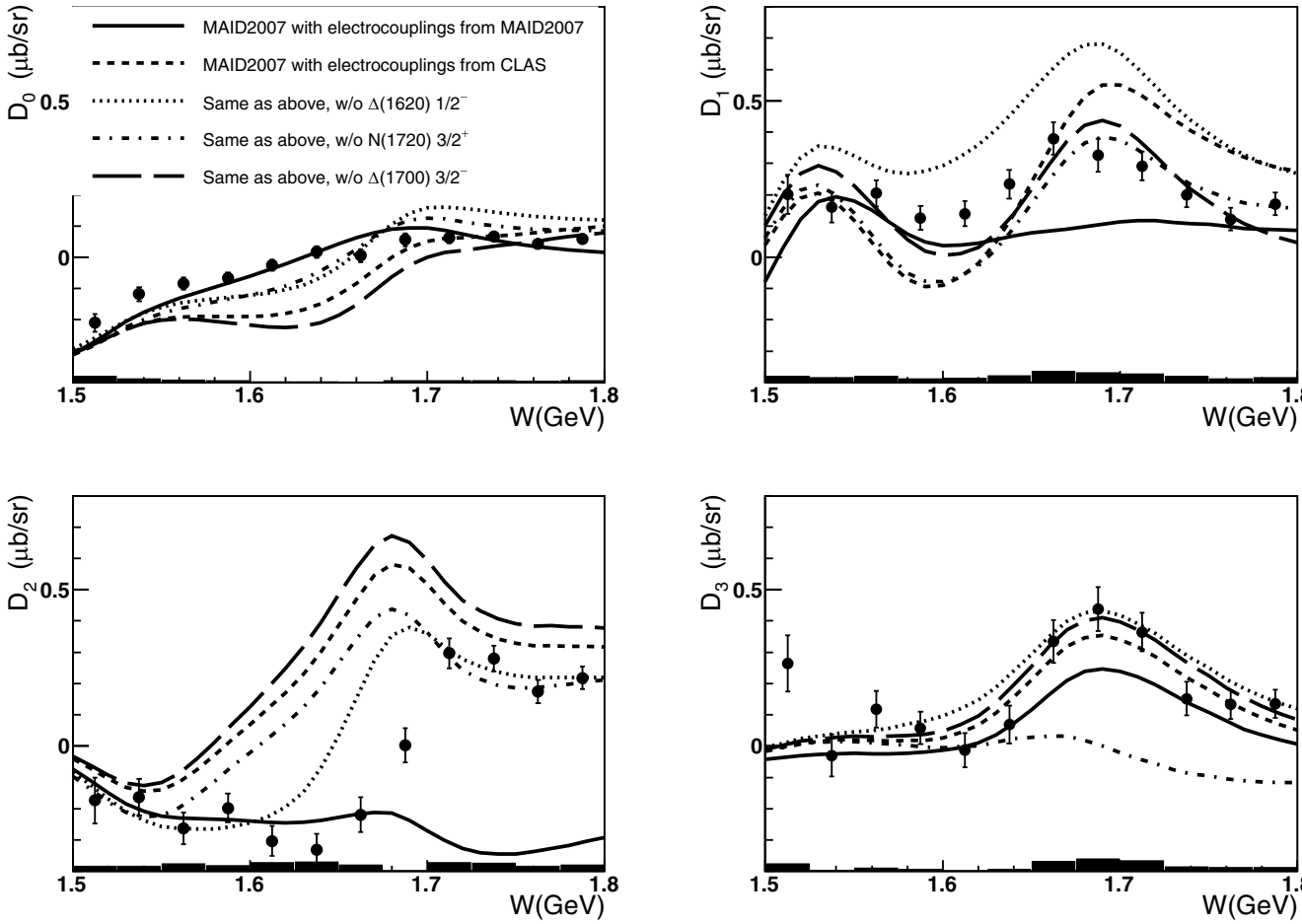


FIG. 3. Legendre moments $D_l(Q^2, W)$ ($l = 0,\ 1,\ 2,\ 3$) of the $\sigma_{LT'}$ structure function from the $\pi^0 p$ electroproduction data at $Q^2 =$ 0.4–0.6 GeV$^2$: $D_0(Q^2, W)$ (top left), $D_1(Q^2, W)$ (top right), $D_2(Q^2, W)$ (bottom left), $D_3(Q^2, W)$ (bottom right). The experimental results are shown by the filled circles with error bars accounting for the statistical uncertainties. The systematic data uncertainties are shown in the bottom part of each plot. The computed $D_l$ moments within the MAID model [27] with the $\gamma_v pN^*$ electrocouplings from Ref. [30] and from Refs. [11,28,29] are shown by the thick solid and dashed lines, respectively. We also show the computed $D_l$ values within the MAID model [27] with the $\gamma_v pN^*$ electrocouplings from Refs. [11,28,29] when the contributions from particular resonances are taken out: $\Delta(1620)1/2^-$ (thin dotted lines), $\Delta(1700)3/2^-$ (thick long-dashed lines), $N(1720)3/2^+$ (thin dash-dotted lines).

other resonances from the CLAS results [11,28,29]. The sensitivity to the particular resonance contributions can be seen in Fig. 3 as the difference between the computed $D_l$ moments when the contributions from all resonances are taken into account (thick dashed lines) and when the contribution from a particular resonance is turned off. All $D_l$ moments demonstrate variations outside the data uncertainties when the $\gamma_v pN^*$ electrocouplings from $\pi N$ electroproduction [30] are replaced by the CLAS results [11,28,29], suggesting sensitivity of the $\sigma_{LT'}$ data to the resonance contributions in these kinematics.

The $D_0$ moment demonstrates sensitivity to the $\Delta(1620)1/2^-$ resonance (see Fig. 3, top left). This sensitivity is due to the multipole contributions of the $D_0$ decomposition:

$$D_0 \sim (5E^*_{3+} - 2E^*_{3-} + M^*_{1-} + M^*_{1+})S_{0+} + E^*_{0+}(S_{3-} - S_{3+}). \quad (5)$$

We are using the well-known notations for the multipoles explained in Ref. [31]. The impact from the $\Delta(1620)1/2^-$ on the $D_0$ moment emerges from the interference between the $S_{0+}$ resonance multipole with the transverse multipoles from the nonresonant contributions, as well as from interference between the resonance $E_{0+}$ transverse and longitudinal multipoles with the nonresonant contributions.

From the $D_1$ multipole decomposition, we found that $D_1$ should be sensitive, in particular, to the contributions from the $\Delta(1700)3/2^-$ and $N(1720)3/2^+$ resonances since the $D_1$ moment contains the products:

$$D_1 \sim -6E^*_{2-}S_{2-} - 6M^*_{2-}S_{2-} + 6E^*_{1+}S_{1+} - 6M^*_{1+}S_{1+}, \quad (6)$$

where the multipole and the multipole conjugated products in the first two terms contain contributions from the $\Delta(1700)3/2^-$ and in the second two terms from the $N(1720)3/2^+$. The expected sensitivities are supported by the data on the $D_1$ moment (see Fig. 3, top right).

At $W$ from 1.65 to 1.70 GeV, the $D_2$ moment evolves rapidly and changes sign (see Fig. 3, bottom left). Making use of the CLAS results on the $\gamma_v pN^*$ electrocouplings

[11,28,29] allows us to reproduce this trend even when the contributions from either the $\Delta(1620)1/2^-$, $\Delta(1700)3/2^-$, or $N(1720)3/2^+$ are turned off.

The $D_2$ moment is sensitive to the $\Delta(1620)1/2^-$ and $N(1720)3/2^+$ resonances. This sensitivity emerges from the following terms in the $D_2$ multipole decomposition:

$$D_2 \sim 12(M^*_{2+} - E^*_{2-})S_{1+} + 6(3E^*_{2+} + 2M^*_{2+})S_{1+} - 15M^*_{1+}S_{2-} + 5(5E^*_{3+} - 2E^*_{3-} + M^*_{3-} - M^*_{3+})S_{0+} + 5E^*_{0+}(3S_{3-} - 4S_{3+}). \quad (7)$$

The $N(1720)3/2^+$ resonance impacts the $D_2$ moments owing to the interference between its longitudinal $S_{1+}$ multipole and the transverse multipoles from the nonresonant contributions, as well as from the interference of the $M_{1+}$ transverse resonance multipole and the longitudinal part of the nonresonant contributions. The $\Delta(1620)1/2^-$ impacts the $D_2$ moment because of the interference between its $S_{0+}$ multipole and transverse nonresonant contributions, as well as due to the interference between the transverse $E_{0+}$ multipole of the resonance and the longitudinal parts of the nonresonant contributions.

The $D_3$ moment is strongly affected by the $N(1720)3/2^+$ resonance (see Fig. 3, bottom right) due to the interference between the $S_{1+}$ multipole for the resonance and the transverse part of the nonresonant processes, as well as because of the interference between the transverse $M_{1+}$ resonance multipole and the longitudinal part of the nonresonant contribution seen in the multipole decomposition of $D_3$:

$$D_3 \sim 18(M^*_{3-} - E^*_{3+})S_{1+} + (34E^*_{3+} - 36E^*_{3-})S_{1+} - 28M^*_{1+}S_{3+}. \quad (8)$$

Studies of the Legendre moment sensitivities to the resonant contributions at $0.6\ \mathrm{GeV}^2 < Q^2 < 1.0\ \mathrm{GeV}^2$ revealed similar features as those observed for the data at $0.4\ \mathrm{GeV}^2 < Q^2 < 0.6\ \mathrm{GeV}^2$ and discussed above.

In summary, the beam spin asymmetries and the $\sigma_{LT'}$ structure functions have become available from the CLAS data on exclusive $\pi^0 p$ electroproduction at $1.5\ \mathrm{GeV} < W < 1.8\ \mathrm{GeV}$ and photon virtualities $0.4\ \mathrm{GeV}^2 < Q^2 < 1.0\ \mathrm{GeV}^2$. These observables for $\pi^0 p$ electroproduction off protons were obtained for the first time at the invariant masses of the final-state hadrons $W > 1.6$ GeV. The Legendre moments $D_l$ ($l = 0$, 1, 2, 3) were determined from fits of the angular dependencies of $\sigma_{LT'}$ in each bin of $W$ and $Q^2$ covered by the measurements. The $D_0$ and $D_1$ Legendre moments demonstrate sensitivity to the electro-excitation amplitudes of the $\Delta(1620)1/2^-$, $\Delta(1700)3/2^-$, and $N(1720)3/2^+$ resonances. Previously, the information on the electro-excitation amplitudes of these excited states was obtained in the studies of $\pi^+\pi^- p$ electroproduction off protons with CLAS [1,29,32]. Combined studies of the exclusive $\pi^+ n$ and $\pi^0 p$ electroproduction channels will provide independent results on the electro-excitation amplitudes of the nucleon resonances in the mass range of $W > 1.6$ GeV. Comparison of the results on the resonance electro-excitation amplitudes from the studies of both $\pi N$ and $\pi^+\pi^- p$ electroproduction will allow us to shed light on the systematic uncertainties in their extraction.

We acknowledge the outstanding efforts of the staff of the Accelerator and the Physics Divisions at Jefferson Lab in making this experiment possible. This work was supported in part by the U.S. Department of Energy, the National Science Foundation (NSF), the Italian Istituto Nazionale di Fisica Nucleare (INFN), the French Centre National de la Recherche Scientifique (CNRS), the Skobeltsyn Institute of Nuclear Physics, the Physics Department at Moscow State University, the French Commissariat pour l'Energie Atomique, the UK Science and Technology Facilities Council, and the National Research Foundation (NRF) of Korea. The Southeastern Universities Research Association (SURA) operates the Thomas Jefferson National Accelerator Facility for the U.S. Department of Energy under Contract No. DE-AC05-06OR23177. This work was supported in part by the Chilean National Agency of Research and Development ANID PIA/APOYO AFB180002. The work is also supported in part by DOE grant DE-FG02-04ER41309.

[1] D. S. Carman, K. Joo, and V. I. Mokeev, Few-Body Syst. **61**, 29 (2020).
[2] I. G. Aznauryan and V. D. Burkert, Prog. Part. Nucl. Phys. **67**, 1 (2012).
[3] V. D. Burkert and C. D. Roberts, Rev. Mod. Phys. **91**, 011003 (2019).
[4] S. J. Brodsky *et al.*, Int. J. Mod. Phys. E **29**, 2030006 (2020).
[5] I. Aznauryan *et al.*, Phys. Rev. C **80**, 055203 (2009).
[6] K. Joo *et al.* (The CLAS Collaboration), Phys. Rev. Lett. **88**, 122001 (2002).
[7] M. Ungaro *et al.* (The CLAS Collaboration), Phys. Rev. Lett. **97**, 112003 (2006).
[8] A. Biselli *et al.* (The CLAS Collaboration), Phys. Rev. C **78**, 045204 (2008).
[9] K. Park *et al.* (The CLAS Collaboration), Phys. Rev. C **91**, 045203 (2015).
[10] N. S. Markov *et al.* (The CLAS Collaboration), Phys. Rev. C **101**, 015208 (2020).
[11] A. N. Hiller Blin *et al.*, Phys. Rev. C **100**, 035201 (2019).
[12] A. N. Hiller Blin, W. Melnitchouk, V. I. Mokeev, V. D. Burkert, V. V. Chesnokov, A. Pilloni, and A. P. Szczepaniak, Phys. Rev. C **104**, 025201 (2021).
[13] C. D. Roberts, EPJ Web Conf. **241**, 02008 (2020).
[14] J. Segovia, Few-Body Syst. **60**, 34 (2019).
[15] I. G. Aznauryan and V. D. Burkert, Phys. Rev. C **92**, 015203 (2015).
[16] I. G. Aznauryan and V. D. Burkert, Phys. Rev. C **95**, 065207 (2017).

[17] I. T. Obukhovsky, A. Faessler, D. K. Fedorov, T. Gutsche, and V. E. Lyubovitskij, Phys. Rev. D **100**, 094013 (2019).
[18] V. E. Lyubovitskij and I. Schmidt, Phys. Rev. D **102**, 094008 (2020).
[19] G. Ramalho and M. T. Pena, Phys. Rev. D **89**, 094016 (2014).
[20] M. M. Giannini and E. Santopinto, Chin. J. Phys. **53**, 020301 (2015).
[21] K. Joo *et al.* (The CLAS Collaboration), Phys. Rev. C **72**, 058202 (2005).
[22] K. Joo *et al.* (The CLAS Collaboration), Phys. Rev. C **70**, 042201 (2004).
[23] A. S. Biselli *et al.* (The CLAS Collaboration), Phys. Rev. C **68**, 035202 (2003).
[24] K. Joo *et al.* (The CLAS Collaboration), Phys. Rev. C **68**, 032201(R) (2003).
[25] B. A. Mecking *et al.*, Nucl. Instrum. Methods Phys. Res., Sect. A **503**, 513 (2003).
[26] CLAS Physics Database, http://clasweb.jlab.org/physicsdb.
[27] D. Drechsel, S. S. Kamalov, and L. Tiator, Eur. Phys. J. A **34**, 69 (2007).
[28] Fit of the Resonance Electrocouplings, https://userweb.jlab.org/~isupov/couplings/.
[29] V. I. Mokeev, EPJ Web Conf. **241**, 03003 (2020).
[30] L. Tiator, Eur. Phys. J. Spec. Top. **198**, 141 (2011).
[31] G. Knochlein, D. Drechsel, and L. Tiator, Z. Phys. A: Hadrons Nucl. **352**, 327 (1995).
[32] V. I. Mokeev *et al.*, Phys. Lett. B **805**, 135457 (2020).